University of South Australia

The Library
www.library.unisa.edu.au

Educating Professionals, Creating and Applying Knowledge, Engaging our Communities

This is the peer reviewed version of the following article:

Turner, CT, Mcinnes, SJ, Melville, E, Cowin, A & Voelcker, NH 2016, 'Delivery of flightless I neutralizing antibody from porous silicon nanoparticles improves wound healing in diabetic mice', *Advanced healthcare materials*, published online 21 November, 2016, pp. 1-13.

which has been published in final form at http://dx.doi.org/10.1002/adhm.201600707. This article may be used for non-commercial purposes in accordance with Wiley Terms and Conditions for self-archiving.

DOI: 10.1002/ ((please add manuscript number))

Article type: Full Paper

Delivery of Flightless I Neutralizing Antibody from Porous Silicon Nanoparticles Improves Wound Healing in Diabetic Mice

Christopher T. Turner,[$] Steven J. P. McInnes,[$] Elizabeth Melville, Allison J. Cowin* and Nicolas H. Voelcker*

Wound Management Innovation Cooperative Research Centre, Future Industries Institute, University of South Australia, Adelaide, South Australia 5001, Australia. *E-mail:* nico.voelcker@unisa.edu.au or allison.cowin@unisa.edu.au

* Joint corresponding authors

[$]These authors contributed equally to this work

Keywords: Porous silicon, chronic wounds, protein therapeutics, flightless neutralizing antibody, diabetes, improved wound healing.

Abstract

Flightless I (Flii) is elevated in human chronic wounds and is a negative regulator of wound repair. Decreasing its activity improves healing responses. Flii neutralizing antibodies (FnAbs) have been developed that decrease Flii activity *in vivo* and hold significant promise as healing agents. However, in order to avoid the need for repeated application in a clinical setting, and to protect the therapeutic antibody from

the hostile environment of the wound, suitable antibody delivery vehicles are required. In this study, the use of porous silicon nanoparticles (pSi NPs) is demonstrated for the controlled release of FnAb to diabetic wounds. pSi NPs were loaded with FnAb achieving loading regimens exceeding 250 μg of FnAb per mg of pSi. FnAb-pSi NPs increased keratinocyte proliferation and enhanced migration in scratch wound assays. Release studies confirmed the functionality of the FnAb with binding to Flii occurring over a 7 d period. Using a streptozotocin-induced model of diabetic wound healing a significant improvement in healing was observed for mice treated with FnAb loaded pSi NPs compared to controls, including FnAb alone. Additionally, FnAb loaded pSi NPs treated with proteases showed intact and functional antibody for up to 7 days post-treatment, suggesting protection of the antibodies from proteolytic degradation in wound fluid. pSi NPs may therefore aid in new therapeutic approaches for the treatment of diabetic ulcers.

1. Introduction

At any point in time approximately 450,000 Australians suffer from a chronic wound, placing an estimated $3 billion burden on the economy.[1] Chronic wounds are defined as any wound that takes longer than 3 months to heal.[2] Diabetic foot ulcers, one of the most prevalent types of chronic wound, affect up to 25% of diabetic patients.[3] The role of diabetes mellitus in chronic skin conditions has been extensively reviewed by Quondamatteo.[4] There is greater than 2,600 diabetic associated amputations per year in Australia,[5] with diabetic ulcers contributing to 85% of all diabetic amputations.[6] Currently, treatment options for these wounds are limited, however, the use of monoclonal antibodies for various diseases is becoming more prevalent.[7]

Despite antibodies being promising agents for improved chronic wound healing, finding ways to effectively deliver these antibodies to the proteolytic environment of a chronic wound remains a hurdle.

Porous silicon (pSi) is a biomaterial that has several unique features making it attractive for use in a wide variety of *in vivo* and *ex vivo* applications.[8] Bulk crystalline silicon is converted into the high surface area and biocompatible pSi by means of anodisation in hydrofluoric acid (HF) solution. A broad range of porous structures can be generated by altering the wafer resistivity, HF concentrations and the applied current densities. The pore size can be tuned in diameter from a few nanometers to a few microns achieving surface areas of up to 800 m^2/g.[8a] pSi degradation is tunable, from days to months,[8b, 9] depending on the pore size and chemistry and produces non-toxic silicic acid upon degradation.[10] pSi has demonstrated *in vivo* biocompatibility in the subconjuctival space of rats[11] and when injected into the vitreous of rabbit eyes.[12] Bimbo *et al.* have also demonstrated the biodistribution of pSi nanoparticles (pSi NPs) administered via oral, subcutaneous and intravenous administration and shown that the pSi NPs do not induce toxicity or inflammatory responses whilst displaying excellent *in vivo* stability in rats.[13] *Ex vivo* applications include optical biosensors that capitalise on the unique optical and photonic properties of the material and have been exploited in the fields of immunology,[14] cancer diagnostics,[15] chronic wound healing[16] and infectious diseases.[17] The ability of pSi to store and release various payloads of small molecular drugs, oligonucleotides or even protein therapeutics has also been demonstrated.[18]

Flightless I (Flii) is a multifunctional protein that regulates cellular mobility, contraction, adhesion, proliferation and cytokine production.[19] Its activity is mediated through interaction with components of the cytoskeleton, modulation of intracellular signaling pathways and regulation of cellular transcription events.[20] Flii is a member of the family of the actin-binding family of proteins that regulate tightly orchestrated cellular processes including lamellipodial crawling of keratinocytes during wound re-epithelialisation,[21] the infiltration of inflammatory cells,[22] and the migration of fibroblasts required for deposition of the extracellular matrix and dermal contraction at the wound site.[19-20, 23] Flii is a negative regulator of the migratory and proliferative events of wound repair.[19] Flii 'over-expressing' mice exhibit larger, less contracted, wounds, reduced cellular proliferation and delayed re-epithelialization.[19] Conversely, Flii-deficient mice have improved epidermal migration and re-epithelialization, and enhanced wound vascularization.[19, 22b] Flii is secreted in response to injury and is present in wound fluid and in the extracellular matrix.[22a] Neutralizing extracellular Flii, using a Flii monoclonal antibody (FnAb), improves healing of acute wounds, diabetic ulcers and burn injuries in murine and porcine models of wound repair[19, 23-24]

Flii is also elevated in diabetic wounds, with double the amount of Flii present in human wounds of ≥ 6 weeks duration compared to acute wounds.[22a] Reducing the activity of Flii using FnAbs is therefore a potential therapeutic option for the treatment of chronic wounds. However, the effectiveness of antibodies in chronic wound care is potentially limited due to the hostile wound environment, primarily due to increased proteolytic activity[25] and altered pH.[26] pSi is predicted to protect

FnAbs from this harmful environment, but also provide a slow release mechanism to deliver sustained antibodies to the wound site.

The use of pSi MPs and NPs to deliver therapeutic payloads to cells and tissues has previously been reported by our laboratory.[27] These *in vivo* studies showed that pSi MPs and NPs are broken down in the extracellular environment and upon degradation release their contents. This mechanism of drug delivery is therefore expected to provide the bulk of the therapeutic effect in diabetic wounds by delivering functional antibodies to "mop up/neutralize' extracellular Flii protein. However, pSi NPs may also facilitate intracellular drug delivery as pSi NPs can also be endocytosed, with recent reports now showing antibody/protein release from the endosome-lysosome network and into the cytosol by various mechanisms.[28] Finally, pSi manufactured as NPs have improved loading capacities than MPs thereby reducing the amount of pSi that would need to be administered to patients. The current study therefore aims to demonstrate the versatility of pSi as a reservoir for FnAb delivery to diabetic wounds. We propose a system where FnAb is delivered from pSi NPs protecting the antibody from the proteolytic wound environment, providing an improved therapeutic delivery system for the treatment of chronic wounds.

2. Experimental

2.1. Chemicals

Hydrofluoric acid (HF) 48% (Merck), dichloromethane (CH_2Cl_2, Labserv, analytical grade, 99.5%), methanol (Merck, analytical grade, 99.5%), acetone (Ajax, analytical grade, 99.5%), and ethanol (Ajax, absolute, 100%) were used without further

purification. N,N-dimethylformamide (DMF, EMD Chemicals, Belgium) was purified *via* standard laboratory protocols including drying over $MgSO_4$ followed by distillation at reduced pressure.[29] Milli-Q water was obtained from an Advantage A10 water purification system provided by Merck Millipore (water resistivity of 18.2 MΩcm at 25 °C, TOC < 5 ppb). Dulbecco's phosphate buffered saline (PBS) solution, streptozotocin (STZ), bovine serum albumin (BSA), o-phenylenediamine dihydrochloride (OPD) substrate, pepsin from porcine gastric mucosa and fluorescein isothiocyanate (97.5%, FITC) were purchased from Sigma Aldrich and used as received. cOmplete, Mini protease inhibitor cocktail tablets and WST-1 were from Roche. Insulin (2 IU Protaphane/Mixtard) was purchased from Novo-Nordisk. Isofluorane (Forthane) was from AbbVie.

2.2 Antibodies and peptides

Affinity purified mouse monoclonal FnAb was prepared in house. Affinity-purified rabbit polyclonal FnAb and Flii peptide conjugated to keyhole limpet hemocyanin (Flii-KLH) were from Mimotopes (Clayton, Victoria, Australia). Mouse monoclonal anti-KLH antibody was obtained from Abcam. Polyclonal goat anti-mouse HRP was obtained from Dako. Murine IgG non-specific antibody (I8765) was obtained from Sigma (St Louis, MO).

2.3. pSi NP preparation

pSi NPs were fabricated from p-type Si wafers (boron-doped, resistivity 0.0008 – 0.0012 Ωcm, <100>) supplied by Siltronix (Archamps, France). The wafer was anodised in an 18 cm^2etching cell in 3:1 HF:ethanol (v/v) solution with a square wave

form comprising an initial current density of 50 mA/cm^2 for 7.3 s and second current density of 400 50 mA/cm^2 for 0.4 s. This two-step cycle was repeated continuously for 1 h, generating a pSi film with alternating low and high porosity layers. The etched layer was removed from the Si substrate via electropolishing in 1:20 HF:EtOH at 4 mA/cm^2 for 4 min and 10 s. Subsequently the pSi membrane was sonicated for 16 h in DMSO to generate chemically oxidised pSi nanoparticles. These nanoparticles were sized by passing through a 220 nm PTFE syringe filter, followed by the collection of the pellet after centrifugation at 22,000 x g. This filtration and centrifugation allowed for the removal of large and small nanoparticles and facilitated the harvest of reasonably uniformly sized NPs that permanently remained in solution.

2.4 Dynamic light scattering

The mean particle size and size distribution of NPs were determined by dynamic light scattering (DLS; ZetasizerNano ZS, Malvern Instruments, Malvern, UK). The analysis was carried out at a temperature of 25°C using NPs dispersed in undenatured 100% ethanol. Every sample measurement was repeated 15 times.

2.5. Electron microscopy

2.5.1. Scanning electron microscopy (SEM)

SEM was performed on a FEI Quanta 450 FEG environmental SEM fitted with an SSD detector, and operated at 30 keV with a spot size of 2 mm. The pSi membrane was carefully cleaved to reveal a fresh cross section before being mounted on a vertically aligned brass bar stuck to an Aluminum SEM stud via conductive carbon tape. To help facilitate the dissipation of charge build-up, samples were coated with 5

nm thick layer of Pt prior to analysis, according to our standard laboratory protocol.[11]

2.5.2. Transmission electron microscopy (TEM)

The transmission electron microscopy (JEOL JEM-2100F-HR) equipped with a field emission gun was operated at 200kV. The bright field images were recorded by CCD camera (GATAN Orius SC1000). After pSi NP's fabrication the pellet was dispersed in 1 mL of EtOH and diluted 1/1000 times before 20 μL was spotted onto a 300 mesh copper Formvar/carbon TEM grid supplied by Electron Microscopy Supplies and allowed to air dry before insertion into the TEM for analysis. Pore size counts were performed manually with the aid of ImageJ. At least 20 pores were measured per image and at least 3 images were counted before the average pore diameter was calculated and presented with plus or minus one standard deviation.

2.6. Infrared spectroscopy

Attenuated total reflectance infrared (ATR-IR) spectra were obtained using a Bruker Hyperion 1000 IR microscope operating with a Bruker Vertex 80 IR spectrometer. The IR microscope was equipped with a liquid nitrogen cooled MCT detector. ATR spectra were collected over 64 scans, with a resolution of 4 cm^{-1}, using a Ge ATR crystal. All spectra were background corrected with an unetched silicon wafer of the same type. Spectra of the pSi layers were recorded and analysed using OPUS version 7.0 software, in the range of 650 - 4000 cm^{-1}. All IR spectra are presented with absorbance normalised to the Si-O peak at approximately 1100 cm^{-1}.

2.7. Fluorescence microscopy

Fluorescence microscopy was performed on an Eclipse 50*i* microscope equipped with a D-FL universal epi-fluorescence attachment and a 100 W mercury lamp (Nikon Instruments, Japan). Fluorescence images were captured with a CCD camera (Nikon Instruments, Japan), using the following fluorescent filters. Blue channel (violet excitation, blue emission): excitation: 385 - 400 nm (bandpass, 393 CWL), dichromatic mirror: 435 - 470 nm (bandpass) and barrier filter wavelength: 450 - 465 nm (bandpass, 458 CWL). Green channel (blue excitation, green emission): excitation: 475 - 490 nm (bandpass, 483 CWL), dichromatic mirror: 500 - 540 nm (bandpass) and barrier filter wavelength: 505 - 535 nm (bandpass, 520 CWL). Red channel (green excitation, orange/red emission): excitation: 545 - 565 nm (bandpass, 555 CWL), dichromatic mirror: 570 - 645 nm (bandpass) and barrier filter wavelength: 580 - 620 nm (bandpass, 600 CWL). Images were analysed using NIS-elements v3.07 software (Nikon Instruments, Japan).

2.8. FnAb loading and release

2.8.1. General experiments

FnAb was aliquoted at 1 mg/mL in PBS and stored at -80 ^{o}C when not in use. The loading of FnAb (1 mg/mL, pH 7.4) into the oxidised pSi NPs (denoted FnAb-pSi NPs) was carried out using a sealed low protein binding Eppendorf tube. After loading the NPs were spun to the bottom of the tubes (30 min at 22,000 x g) and rinsed with PBS (pH 7.4, 15 min) to remove the weakly adsorbed antibody. The amount of protein loaded was determined from UV-Vis measurements (NanoDrop

2000 Spectrometer, Thermo Scientific) of the supernatant before and after incubation with the pSi NPs. The average loading of all pSi NP preparation used during this study was 268 ± 35 μg of FnAb per mg of pSi. For each experiment with antibody-loaded pSi NPs, the loading regime is mentioned specifically below.

2.8.2. Release experiments

FnAb (1 mg/mL) was labeled with fluorescein isothiocyanate (FITC) for 4 h in a sodium carbonate buffer (100 mM, pH 9.5). After labeling the labeled protein was recovered using a Vivaspin 2 10,000 MWCO spin tube (Sartorius Stedim) according to the manufacturer's instructions. This FITC labeled protein was then added to unlabeled FnAb at a known ratio and this solution was used to load pSi NPs as outlined above. Release was then monitored at 25 ^{o}C on an Agilent Technologies Cary Eclipse fluorimeter fitted with a Peltier temperature control system with a PMT of 650 V and excitation and emission slit widths of 5 nm. The emission was monitored at 525 nm and the excitation was performed at 490 nm. Data was recorded in an automated kinetic mode every 8 h for 7 d. The FITC signal was calibrated against a calibration curve constructed from dilutions of the FITC labeled FnAb stock solution.

2.9. Flii sandwich ELISA (pSi-bound FnAb detection)

A sandwich enzyme-linked immunosorbent assay (ELISA) was performed to detect functional FnAb bound to either pSi particles or the well surface of a 96-well plate (assay control; Greiner) **(Figure S1A, B)**. Here, pSi MPs were used instead of pSi NPs as excess unbound antibody is simply removed (i.e. pSi MPs can be centrifuged into a pellet), thereby reducing assay interference. Also, rabbit polyclonal FnAb was

used instead of mouse monoclonal FnAb to prevent species cross-reactivity with the mouse α-KLH antibody. Both FnAb antibodies were raised to the same peptide sequence and displayed similar binding kinetics by ELISA.

To capture FnAb to the 96-well plate well, FnAb, diluted to 10 µg/mL in 0.1M $NaHCO_3$, was added at 50 µL/well and incubated for 12 h at 4ºC. Wells were washed five times with 200 µL/well of 0.02 M Tris/HCl, 0.25 M NaCl buffer, pH 7, using a microtitration plate washer (ADIL instruments). To quench non-specific binding, wells were blocked by the addition of 200µL 1% (w/v) BSA in 0.02M Tris/HCl, 0.25M NaCl buffer, pH 7, for 4 h at 20 °C. Wells were aspirated and incubated with 100 µL/well block buffer containing 10 µg/mL Flii-KLH, for 12h at 4ºC. Wells were washed five times then incubated with 100 µL/well block buffer containing 10 µg/mL mouse α-KLH antibody, for 12h at 4ºC. Another round of washed were performed before incubation with α-mouse HRP diluted 1/500 in block buffer for 1 h at 20ºC. Unbound antibody was again removed by washing. OPD substrate (100 µL) was added to each well and incubated at 20 °C for 20 min to allow color development. The optical density of each well was measured at 450 nm on an automated ELISA plate reader (SunriseTM, Tecan Group Ltd., Australia).

The sandwich ELISA protocol involving FnAb being bound to pSi particles was similar to when FnAb was bound to the 96-well plate. The major difference was the addition of 1 mg FnAb-pSi MP per well to each 96-well plate well prior to the addition of FnAb (35 µg FnAb per mg pSi). Also, pSi was removed for the wash steps and then added back to unused wells for the following steps of the ELISA. Briefly, pSi MPs particles were decanted, centrifuged at 8,000 g for 5 min at 4 ºC, the

supernatant was discarded, and the pSi pellet resuspended in 200 µL wash buffer. The OPD color change step involved the buffer being removed from the well, centrifugation at 8,000xg for 5 min to pellet the pSi particles, and finally the supernatant decanted back into unused wells for substrate detection on the plate reader.

2.10. FnAb detection ELISA (release from FnAb-pSi NPs)

A direct ELISA to detect FnAb was performed as previously described **(Figure S1C)**.[24b] Briefly, a 100-µL aliquot of Flii peptide at a concentration of 10 µg/mL in 0.1 M $NaHCO_3$, pH 8.5, was added to each well of a polyvinylchloride plate and incubated overnight at 4°C. Unbound peptide was aspirated from each well and the wells were washed three times with 0.02 M Tris/HCl, 0.25 M NaCl buffer, pH 7, using a microtitration plate washer (ADIL instruments). Any remaining reactive sites in the wells were blocked by the addition of 200µl of 1% (w/v) BSA in 0.02M Tris/HCl, 0.25M NaCl buffer, pH 7, for 4 h at 20°C. Supernatant samples were centrifuged at 10,000 g for 30 min at 4ºC to remove pSi NPs, serially diluted in 1% (w/v) BSA in 0.02 M Tris/HCl, 0.25 M NaCl buffer, pH 7, and 50 µL was added to each ELISA well overnight at 4°C. Purified FnAb was also serially diluted, ranging from 12.5-50 µg/mL as a calibration curve. Unbound antibody was then aspirated and the plates were washed three times using a microtitration plate washer. Wells were then incubated with 100 µL of peroxidase- conjugated goat anti-mouse immunoglobulin at a 1/600 dilution in 0.02 M Tris/HCl, 0.25 M NaCl, pH 7, for 1 h at 20°C. Any unbound antibody was removed and the plate washed three times using a microtitration plate washer. OPD substrate (100 µL) was added to each well and incubated at 20°C for 20 min to allow color development. The optical density of each

well was measured at 450 nm on an automated ELISA plate reader (Sunrise^{TM}, Tecan Group Ltd., Australia). The concentration of FnAb in each sample was determined by interpolation through the calibration curve.

2.11. Protein assays

Protein and antibody was quantified by NanoDrop UV-Vis (Thermo Scientific, Wilmington, USA) as per the manufacturer's instructions.

2.12. *In vitro* wound healing assay

The electrical properties of confluent and wounded keratinocytes was examined using Electric Cell-sensing Impedance Sensing (ECIS) as previously described,[30] applying the scratch wound assay function (Applied Biophysics, Troy, NY, USA).[31] Briefly, primary keratinocytes were seeded into an 8W2X1E ECIS Cultureware Array (Applied Biophysics, Troy, NY, USA) and cultured until confluence, as determined by a plateau in the impedance signal at 24,000 Hz. FnAb-pSi NPs (290 µg FnAb per mg pSi) were diluted in fresh culture medium, sonicated for 5 min, then added to the culture wells, with each well receiving an equivalent of 20 µg FnAb. The cell impedance signal was tracked for 10 min before the array sensors were wounded at 2,500 µA, 48,000 Hz for 30 s, with effective wounding observed as a drop in impedance signal. The recovery of the wounded area was determined in real time by impedance, with recovery defined as the time taken for the signal to plateau.

2.13. Cell proliferation assay

Cell proliferation assays were performed using the metabolic substrate WST-1 according to the manufacturer's protocols (Roche Applied Science, Munich,

Germany). FnAb-pSi NPs (290 µg FnAb per mg pSi) were diluted in fresh culture medium, sonicated for 5 min, then added to the culture wells, with each well receiving an equivalent of 20 µg FnAb.

2.14. Animal studies

All experiments were approved by the Adelaide Children Youth and Women's Health Service Animal Care and Ethics Committee following the Australian Code of Practice for the Care and Use of Animals for Scientific Purposes (AE 973/03/17 and AE 991/12/17). Six mice were included per treatment group, with only female mice included in the study.

2.14.1. Murine surgical techniques

Mice were anaesthetised with inhaled isofluorane, and the dorsum shaved and cleaned with 10% (w/v) povidine iodine solution. Incisional wounds were performed on the non-diabetic wild-type Balb/c mice (acute wounds). These wounds 1) provided a direct comparison to previous studies[19]; and 2) provided a rapid healing model, which is simple and relatively fast to perform. STZ-induced diabetic mice received excisional wounds (diabetic wounds) as; 1) they take longer to heal than incisional wounds, providing a larger window for therapeutic effectiveness to be evaluated, and; 2) previous studies showed increased protease concentration in excisional wound models.[32] In the non-diabetic mice, two equidistant 1 cm full-thickness incisions were made through the skin and panniculus carnosus using fine scissors on the flanks of the animals extending 3.5 - 4.5 cm from the base of the skull, 1 cm on either side of the spinal column. In the diabetic mice, equidistant 6 mm full-thickness excisions were made using punch biopsy. Incisional and excisional wounds were left to heal by

secondary intention (i.e. the wound edges were not closed by sutures). Digital photographs were taken of the wounds daily. A ruler was aligned next to the wound to allow direct wound area and wound gape measurements to be made. Wounds were harvested at either 7 (acute and diabetic wounds) or 14 d (diabetic wounds only) and were bisected. One half was fixed in 10% (v/v) buffered formalin and processed so that the midpoint of the wound was sectioned and compared between groups. The other half was micro-dissected to remove any contaminating normal, unwounded skin and snap-frozen in liquid nitrogen for protein extraction.

2.14.2. Diabetic mouse model

Diabetes was induced using multiple low-dose STZ.[33] STZ is toxic to the pancreatic β-islet cell, rendering the mouse unable to produce an adequate amount of insulin.[34] Briefly, female 10-14 weeks old Balb/c mice were administered one IP injection of STZ for five consecutive days (STZ: 50 mg/kg, Sigma) in citrate buffer, pH 7. Mice were fasted for four hours before STZ injection.

Non-fasting blood glucose levels (BGL) testing commenced 3 weeks post-STZ injection by tail vein sampling. To maintain body weight and prevent ketoacidosis after 4 weeks of the last STZ injection animals with BGL > 15 mmol/L were administered subcutaneous injections of insulin (2 IU Protaphane/Mixtard insulin, Novo-Nordisk). Using this regimen, the mice were maintained for a further 6 weeks, then wounded. Mice maintaining a BGL > 15 mmol/L for a minimum of 2 weeks were classified as diabetic, with all others excluded from the trial Cutaneous wounds in this mouse model result in a delayed healing outcome.[35] This model represents the

best alternative to a true chronic wound healing model which is not available due to animal welfare reasons.

2.14.3. Delivery of FnAb-pSi NPs to mice wounds

At time of injury, each wound was injected intradermally at the wound margin, using a 21G gauge needle to deliver a total volume of 100 µL. Incisional wounds received 50 µL to each side, whilst excisional wounds received 25 µL in four equidistant locations around the wound margin. All samples were diluted in phosphate buffered saline (PBS), pH 7.2, with pSi NP samples sonicated for 5 min prior to injection. A total of 50 µg antibody was delivered to each wound, with the amount of administered pSi-NP dependent on the efficacy of antibody loading.

2.14.4. Histology, immunohistochemistry and image analysis

Histological sections (4 µm) were cut from paraffin-embedded fixed tissue, with sections stained with haematoxylin and eosin as previously described.[36]

2.15. Protease treatment of FnAb-pSi NPs

FnAb-pSi NPs were treated with pepsin, a protease that fragments IgG, to evaluate the protective properties of pSi. Using an orbital shaker (Ratek, Adelab Scientific), FnAb-pSi NPs (283 µg FnAb per mg of pSi) were incubated with pepsin (0.8% w/v) in 10 mM HCl, pH 2.5, for 90 min at 37 ºC. As a negative control, an equivalent amount of FnAb-pSi NPs was incubated under the same conditions but in the absence of pepsin. Samples were centrifuged at 8,000 g in an ultracentrifuge (Heraeus Fresco 21,Thermo Scientific) for 5 min to pellet the pSi NPs, with the supernatant collected for analysis. To remove residual pepsin, pSi NPs were resuspended in 500 µL phosphate buffer,

pH 7, mixed well then re-spun. Following three rounds of washing, pSi NPs were resuspended in phosphate buffer, pH 7, containing 200 µg/mL BSA and protease inhibitors. Samples were incubated for 2 weeks at 25 ºC, with the buffer replaced daily and supernatants retained for further analysis. To confirm pepsin effectively fragmented FnAb, 100 µg of free FnAb (i.e. not associated with pSi) was also incubated with and without pepsin in 10 mM HCl, pH 2.5, for 90 min at 37 ºC. Although the release experiments in this study were performed at 25ºC (similar to wound environments), all pepsin digestions were performed at 37ºC to allow maximal antibody fragmentation.

2.16. SDS PAGE gel electrophoresis

Non-denatured sodium dodecyl sulphate-polyacrylamide gel electrophoresis (SDS-PAGE) was used to estimate antibody fragmentation[37] in response to pepsin treatment of FnAb-pSi NPs. Samples were prepared in SDS running buffer in the absence of 2-mercaptoethanol and there was no boil step performed. The gel, containing 10% (w/v) SDS, was run at 100 V for 60 min. The gel was excised and stained with Coomassie blue for 60 min, then de-stained for 2 h.

2.17. Statistical analysis

Statistical differences were determined using the Student's t-test or an ANOVA. For data not following a normal distribution, the Mann-Whitney U-test was performed.[38] A P value of less than 0.05 was considered significant.

3. Results

3.1. Particle fabrication and characterization

pSi NPs were produced via anodisation of a boron-doped Si p^{++}-type wafers in a mixture of aqueous hydrofluoric acid (HF) and ethanol in a Teflon cell with a platinum counter electrode. The perforated structure was visualised by SEM (**Figure 1i**). The approximate thickness of the perforated layer was 31.3 µm while the pSi NP layer and the perforation layer measured approximately 176 nm and 37 nm in thickness, respectively. After anodization, the resulting pSi film was lifted off the Si wafer by electropolishing in dilute HF solution. The pSi film was fractured by ultra-sonication into pSi NPs, which were then filtered through a 220 nm filter membrane. After filtration the pSi NPs were then centrifuged at 22000 × g to remove small non-porous pSi NPs generated from the perforation layers. The resulting pellet of pSi NP was re-dispersed in ethanol. TEM images (**Figure 1**) of the obtained pSi NPs show mesoporous nanoparticles with sizes in the range of 161 ± 58 nm and a pore size of 33 ± 7 nm. DLS gave a nanoparticle size of 149 ± 25 nm in good agreement with the TEM based size measurements.

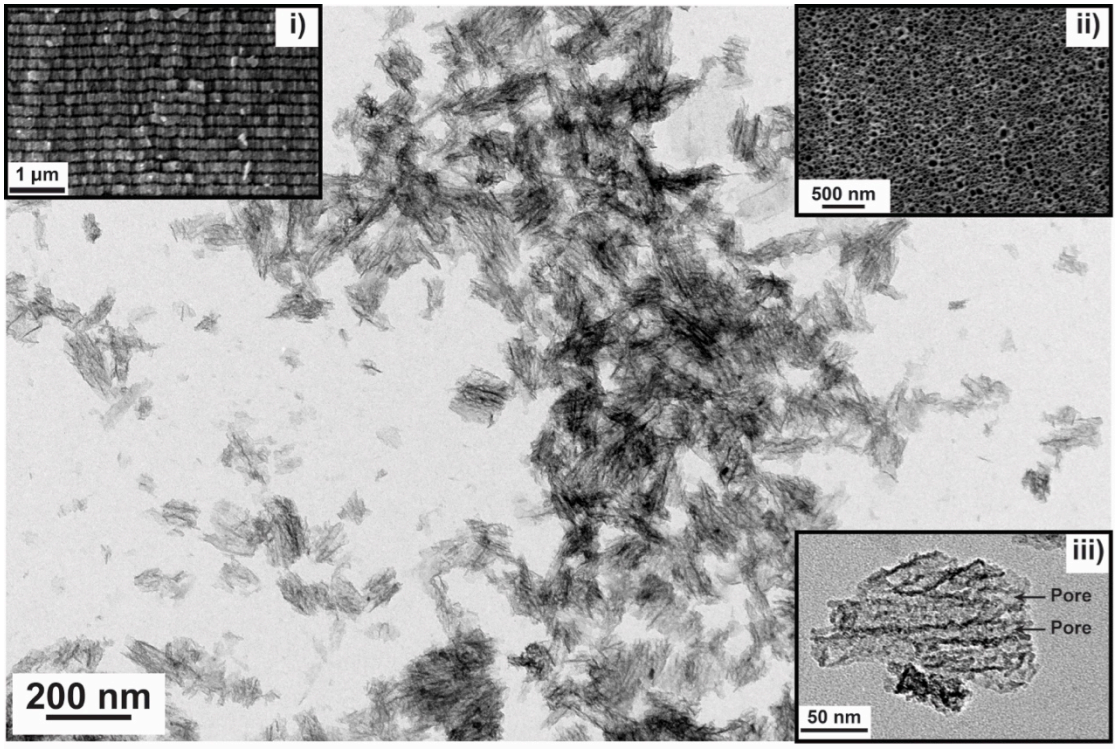


Figure 1: Typical TEM micrograph of pSi NPs. Inset i shows the cross-section SEM image of the perforated membrane structure prior to sonication, inset ii shows the top down SEM image of pSi NP layer and inset iii shows an individual pSi NPs characterised by TEM.

3.2. pSi NP loading with FnAb

All FnAb loadings were performed with 1 mg/mL solutions of FnAb at pH 7.4 in PBS. pSi NPs were highly efficient at loading FnAb and were able to take an average loading of 268 ± 35µg of FnAb per mg of pSi. All loadings, for each individual batch of NPs used throughout this manuscript were analysed by UV-Vis before use, allowing accurate loading results to be calculated for each sample and experiment.

The infrared spectra of ozone-oxidised pSi **(Figure 2, pSi-Ox)** showed a strong and broad peak centred at 1080 cm^{-1} due to asymmetric stretching vibrations of Si-O-Si

surface bridging groups. It is important to note that the main Si-H_x stretching region at 2100 cm^{-1} has been completely removed via the oxidation process. The shoulder located at approximately 1150 cm^{-1} can be attributed to the stretching of O-Si-O surface oxide species.[39] After loading of FnAb into the oxidised pSi film **(Figure 2, pSi-Ox + FnAb)**, the spectra still showed strong characteristic peaks from the pSi-Ox surface in addition to new peaks at 1560 cm^{-1} and 1651 cm^{-1} for the amide I and II vibrations. Hence, FnAb was successfully loaded into the pSi substrate. Our earlier work with Infliximab has shown that large antibodies are able to penetrate throughout pSi networks up to 80 µm thick.[27] pSi NPs without FITC-FnAb did not show any autofluorescence in the green channel prior or post loading with FITC-FnAb (**Figure S2 and S3**).

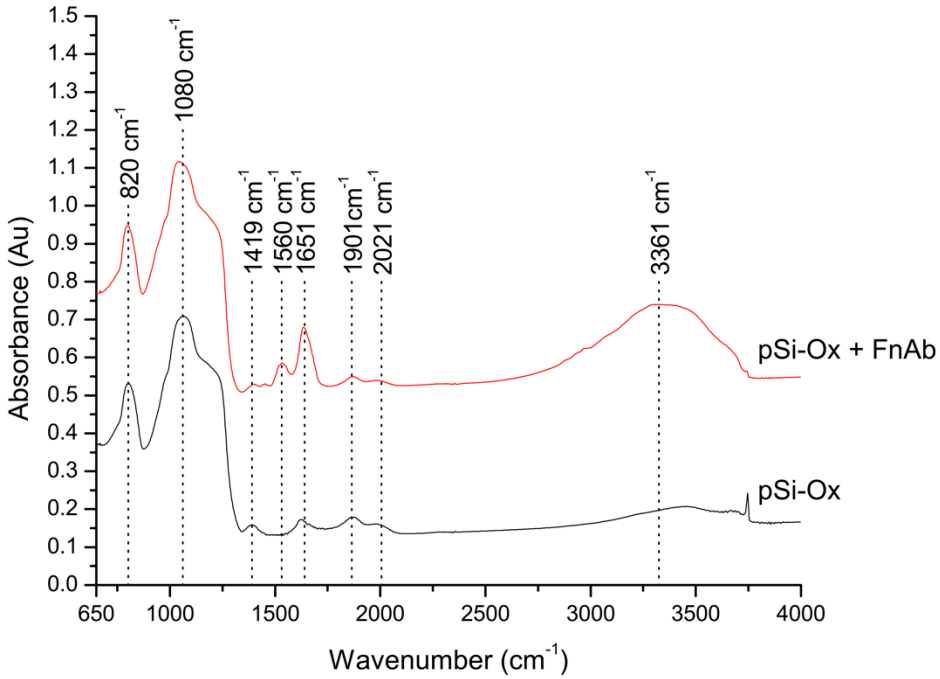


Figure 2:IR spectra of oxidised pSi NPs and oxidised pSi loaded with FnAb.

FITC labeled proteins were monitored for their release kinetics from pSi NPs *via* fluorescence **(Figure 3A)**. Over the course of 7 d, approximately 86.3% of the antibody was released, the kinetics closely match Higuchi model (R^2 = 0.998). The Higuchi model is an empirical model commonly used to describe the release kinetics of drugs from insoluble porous materials.[40] It is well established and commonly used for modeling drug release from matrix systems. The model is based on a square root of a time dependent process of Fickian diffusion. The Ritger-Peppas model also showed a very good fit (R^2 = 0.997) and the n values was above 0.5 (indicating that the FnAb was released according to non-Fickian (anomalous) diffusion).[9a] Loading was also qualitatively confirmed by fluorescence microscopy of dried FITC-FnAb loaded pSi NPs **(Figure 3B)**. An ELISA showed that FnAb, when bound to pSi, retained functionality of binding to the Flii-peptide (**Figure 3C)** with minimal non-specific cross reactivity.

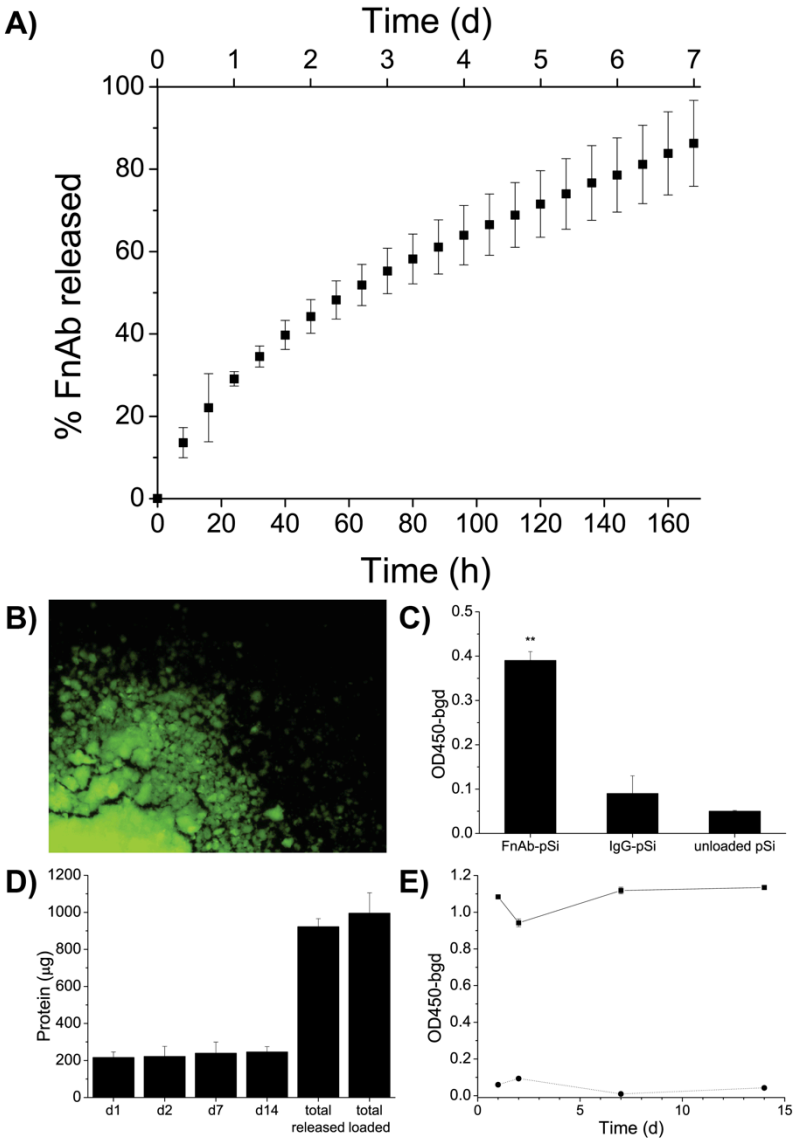


Figure 3: A) Release curves of FITC labeled FnAb from pSi NPs in PBS at 25 ºC,B) fluorescence micrograph of pSi NPs loaded with FITC labeled FnAb (FITC-FnAb-pSi NPs) dispersed on a glass slide. C) Sandwich ELISA to detect functional FnAb bound to pSi particles (FnAb-pSi). pSi was also loaded with non-specific IgG (IgG-pSi) or remained unloaded (unloaded pSi). Data presented as signal at 450 nm minus background. D) Detection of total FnAb released from pSi NPs when incubated in PBS/BSA buffer for 2 weeks at 25 ºC. The column showing total loaded protein was determined by measuring total protein in the loading buffer before and after the initial load step. The column showing total released protein was evaluated by combining the

protein estimates from each individual supernatant sample. E) A direct ELISA was used to detect functional FnAb (■) in the supernatant samples (i.e. FnAb released from pSi NPs), with data presented as signal at 450 nm minus background. Supernatant was also collected from unloaded pSi NPs (●) and analysed by ELISA. Each supernatant sample contained a similar amount of FnAb. All data presented as mean +/- one standard deviation (n=3). * $P < 0.05$. ** $P < 0.005$.

3.3. Activity testing of released FnAb

FnAb released from pSi NPs was collected at day 1, 2, 7 and 14, and tested by FnAb functional detection ELISA. **Figure 3D** shows that equivalent amounts of FnAb was released at each time point, with 93% of total loaded FnAb released after 14 d. Released FnAb present in the supernatant at each time point was demonstrated to successfully bind to the Flii peptide (**Figure 3E**), indicating FnAb retained its functionality for up to 14 d. There was negligible signal detected in the supernatant from unloaded pSi NPs, whilst the pSi degradation by-products were shown to not interfere with the ELISA assay (**Figure S4)**.

Keratinocytes and fibroblasts treated with FnAb in solution show improved scratch wound closure, cell migration and proliferation.[19] To demonstrate FnAb released from pSi NPs retained its functionality, primary keratinocytes at confluence were treated with FnAb-pSi NPs, then electrically wounded (ECIS wound healing assay), with recovery was determined by impedance measurements (**Figure 4A, B**). Cells treated with FnAb-pSi NPs showed a 25% increase in impedance recovery compared to cells treated with unloaded NPs ($P < 0.005$ for > 1 h in time). There was no difference in impedance signal between unloaded pSi NP-treated cells and those wells

with a media only control (data not shown), indicating that unloaded pSi had no effect on wound healing. A WST-1 assay was performed to determine the effect of FnAb-pSi NPs on cellular proliferation (**Figure 4C**). Sub-confluent keratinocytes incubated with FnAb-pSi NPs showed a significant increase in proliferation at 48 h compared to cells treated with unloaded NPs ($P < 0.05$).

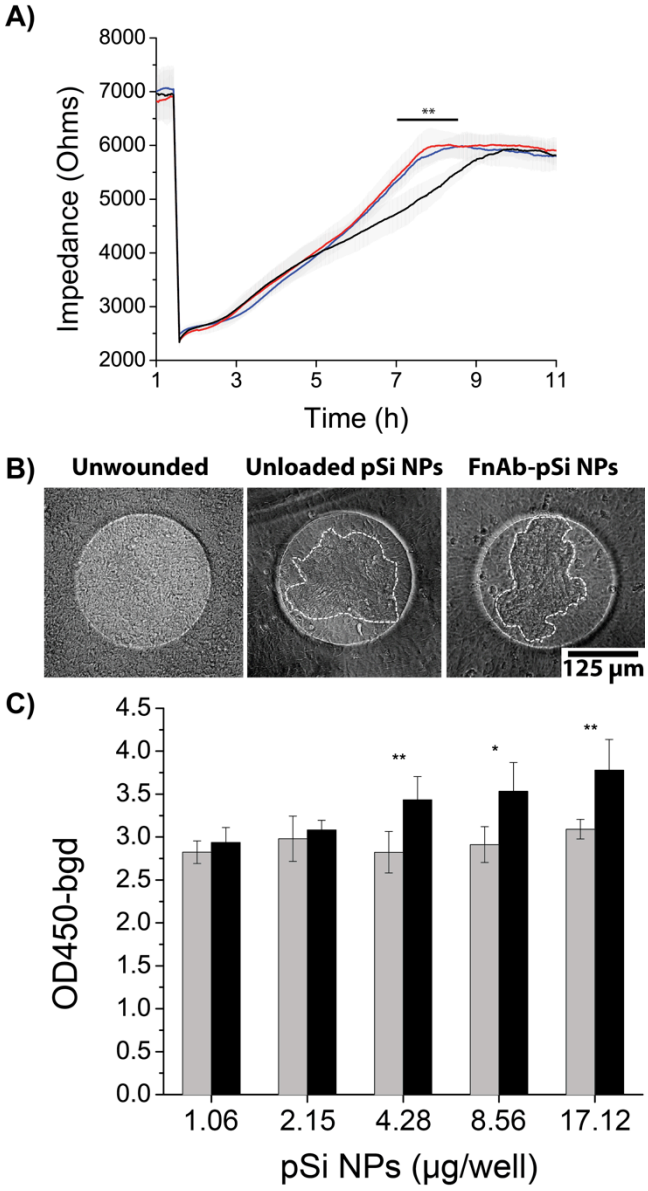


Figure 4: Effect of FnAb-pSi NPs on wound healing and cell proliferation. ECIS wound healing assay (A,B). A) Primary keratinocytes were grown to confluence in 8W2X1E arrays, before addition of FnAb-pSi NPs. The ECIS array was incubated for

10 min to allow the impedance signal to equilibrate before electrical wounding at 2,500 µA and 48,000 Hz for 30 s (at t = 1.5 h). Cells recovery was then monitored by impedance at 24,000 Hz for 10 h. Cells were treated with FnAb-pSi NPs (25 µg/well NP @ 292 µg FnAb/mg NP; red, 12.5 µg/well NP; blue) and unloaded pSi NPs (black). Three array sensors were wounded for each treatment group, with data presented as mean +/- one standard deviation. B) Photographs of the array sensors, at t = 7 h, showing unwounded cells (outside the dotted line), and wounded cells (inside the dotted line) treated with FnAb- or unloaded pSi NPs. The infiltration of keratinocytes into the wound area, which was more pronounced in the FnAb-NP treated cells, corresponds to an increased impedance. The scale bar is 125 µm. C) WST-1 proliferation assay where primary keratinocytes were seeded at 5×10^4 cells/ml and incubated for 24 h, washed with PBS, then treated with FnAb-pSi NPs (black bars) or unloaded pSi NPs (grey bars) over a mass range of 1.06 - 17.12 µg of pSi/well (giving an FnAb concentration of 3.1, 6.3, 12.5, 25 and 50 µg/well). Data presented as mean +/- one standard deviation (n=6). * $P < 0.05$. ** $P < 0.005$.

3.4. *In Vivo* testing - 7 day incisional mouse model wound trial

Acute incisional wounds in wild-type mice were treated with FnAb-pSi NPs and mIgG-pSi NPs, involving a single dose at the time of injury. The dose of FnAb selected for this study corresponded to the optimal concentration used in another wound trial, where FnAb was administered alone (i.e. no pSi delivery vehicle),[19] and was supported by published release data showing that functional antibody was efficiently released from pSi MPs into wound fluid.[27] The wound area for all mice increased in the first 24 h as a result of accumulated wound exudate transiently

expanding the wound margin. Wounds treated with FnAb-pSi NPs had significantly smaller wound areas at day 6 (40%) and 7 (45%) than those treated with mIgG-pSi NPs ($P < 0.005$, **Figure 5A**). The rate of wound closure is particularly important in the healing of wounds as it helps to reduce the possibility of infection which is a leading course of impaired healing and scar formation. This improvement in the rate of wound closure following treatment with FnAb would be considered clinically relevant. Whilst the wound gape at day 7 for FnAb-pSi NP treated wounds was significantly smaller than for mIgG-pSi NPs or unloaded pSi NPs, the small improvement compared to free FnAb without pSi NPs was not statistically significant in this acute model (**Figure 5B**). This lack of significance between the free FnAb treated acute wounds and for FnAb-pSi NP treated wounds is likely due to the acute wound environment which do not have the same proteolytic environment of a chronic wound. However, this animal trial was important in establishing that FnAb was released from pSi and retained its functionality. In addition, no statistically significant difference was observed in wound gape between mice treated with mIgG-pSi NPs, mIgG alone and unloaded pSi NPs (**Figure 5B, C**). Analysis of tissue sections at day 7 by hematoxylin and eosin staining confirmed the macroscopic wound measurements (**Figure 6**).

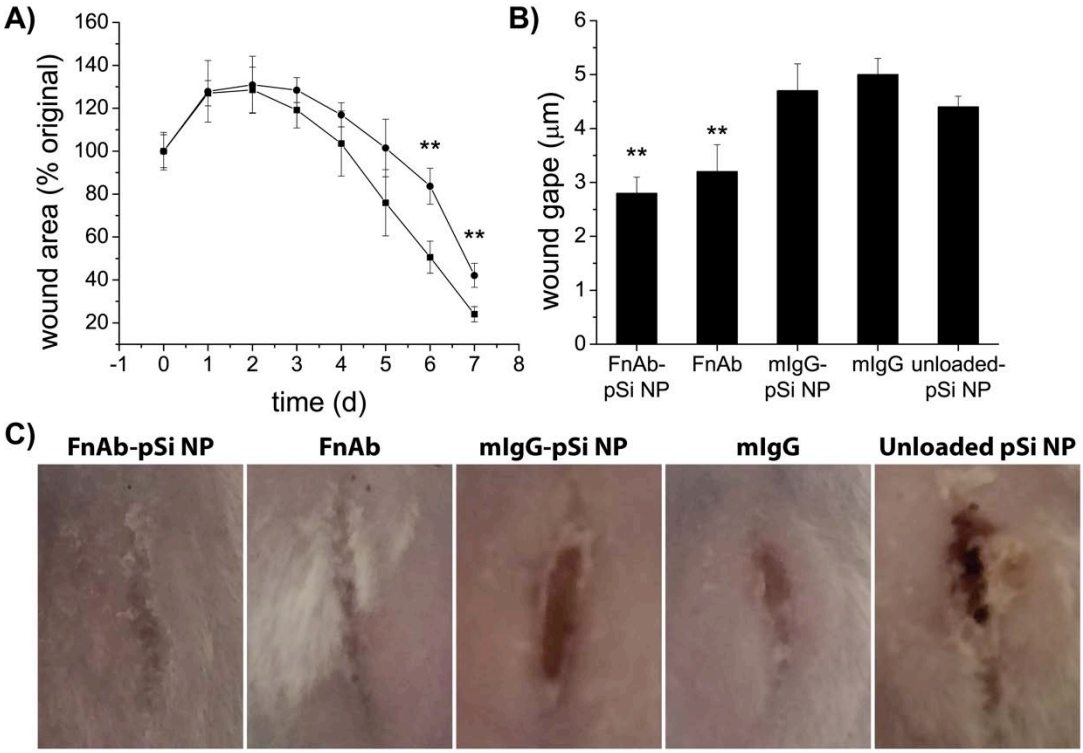


Figure 5: Macroscopic analysis of incisional wound trial in healthy wild-type mice. Wounds were treated with intradermal injections of FnAb-pSi NPs (■) or mIgG-pSi NPs (●) at the time of injury (A). A) Wound gape calculated as a % of original wound area. Each wound was treated with the equivalent of 50 µg of FnAb or mIgG. B) At day 7, wound gape was also determined in mice treated with FnAb alone, mIgG alone and unloaded pSi NPs. C) Images of the incisional wounds at day 7. Each treatment group contained six mice, with two wounds per mouse. Images (C) were representative of each treatment group. * $P < 0.05$. ** $P < 0.005$.

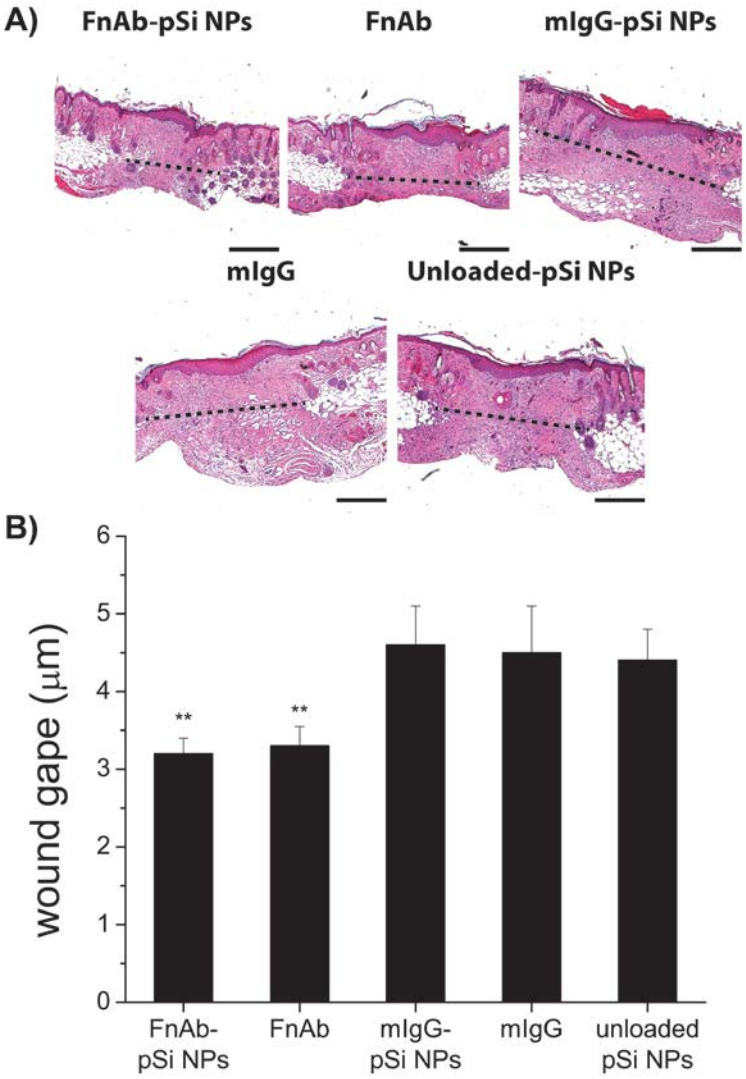


Figure 6: Microscopic analysis of incisional wound trial in healthy wild-type mice. Wounds were treated with a single intradermal injection of FnAb-pSi NPs, FnAb alone, mIgG-pSi NPs, mIgG alone or unloaded pSi NPs at the time of injury. Mice were humanely killed at day 7 post-surgery, with wound tissue sectioned, stained with haematoxylin and eosin (A) and wound gape measured (B). The dashed lines in panel a show the width of the wounded dermis in each tissue section. Each wound was treated with the equivalent of 50 µg of FnAb or mIgG. Each treatment group contained six mice, with two wounds per mouse. Images in (A) were representative of

each treatment group. ** $P < 0.005$ compared to mIgG-pSi NP treated controls. Scale bar is 100 μm.

3.5.FnAb-pSi NPs improve wounding in diabetic mice

FnAb-pSi NPs were administered to excisional wounds in diabetic mice, involving a single intradermal dose at the time of injury (**Figure 7**). The wound area in FnAb-pSi NP treated mice was significantly smaller than mIgG-pSi NP control treated wounds at days 6 and 7 ($P < 0.005$), with an improvement in the rate of wound healing leading to wounds closing approximately 2 d earlier (equivalent to 18% faster) (**Figure 7A**). FnAb-pSi NP treated mice wounds at day 7 were 30% smaller wounds at day 7 than when FnAb was administered alone ($P < 0.05$) (**Figure 7B, C,** and **Figure 8**). There was no difference in wound area between mice treated intradermally with mIgG-pSi NPs, with these wounds re-epithelialised by day 11 or 48 h later than those treated with FnAb-pSi NP. At day 14, all wounds were the same size, indicating that although FnAb treated wounds healed more rapidly there was no effect on remodeling and scar formation. Interestingly, no difference in wound area was seen between treatment with FnAb alone without pSi NPs compared to FnAb and pSi NPs when added together (i.e. NPs were not loaded with antibody prior to administration).

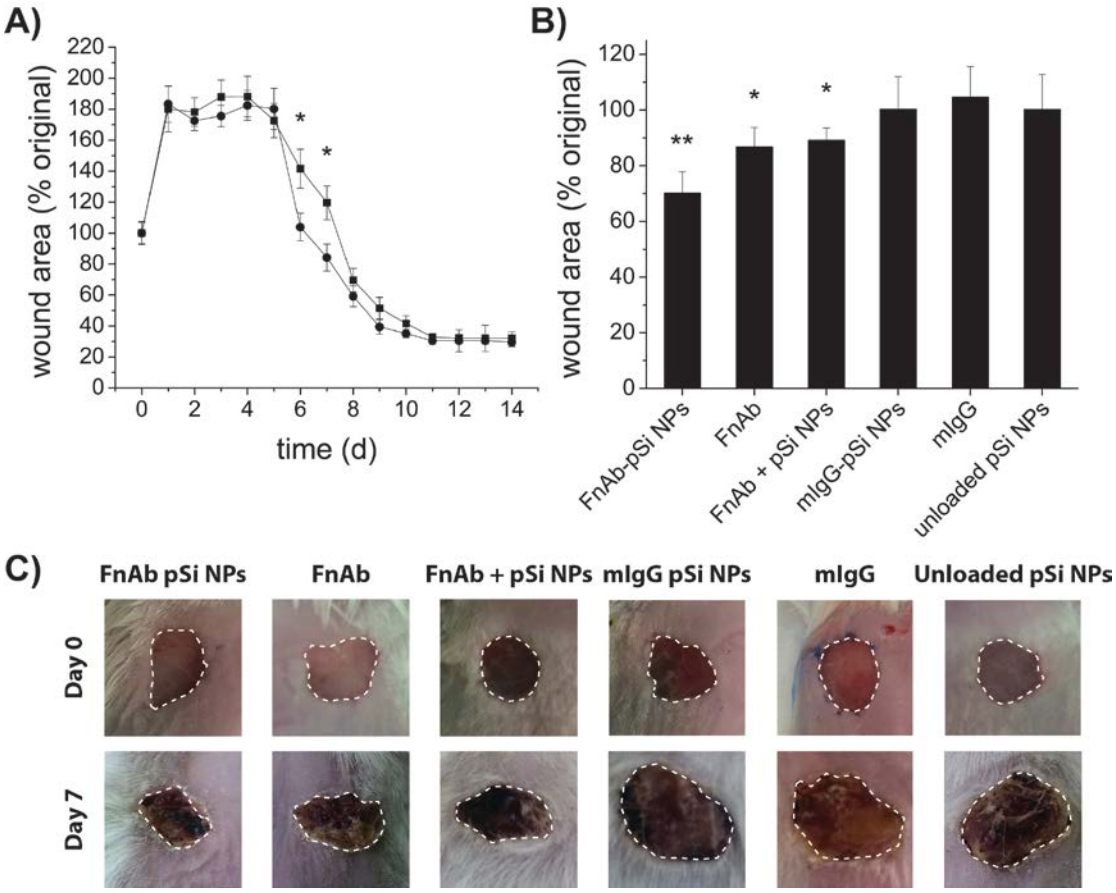


Figure 7: Macroscopic analysis of excisional wound trial in diabetic mice. Wounds were treated with intradermal injections of FnAb-pSi NPs (●) or mIgG-pSi NPs (■) at the time of injury (A). Each wound was treated with the equivalent of 50 µg of FnAb or mIgG. At day 7, wound gape was also determined in mice treated with FnAb alone, mIgG alone and unloaded pSi NPs (B, C). Wound area calculated as a % of original wound area. Each treatment group contained six mice, with two wounds per mouse. Images (C) were representative of each treatment group. The dotted line indicates the wound margin at day 7.* $P < 0.05$, ** $P < 0.005$ compared to mIgG-pSi NP treated controls.

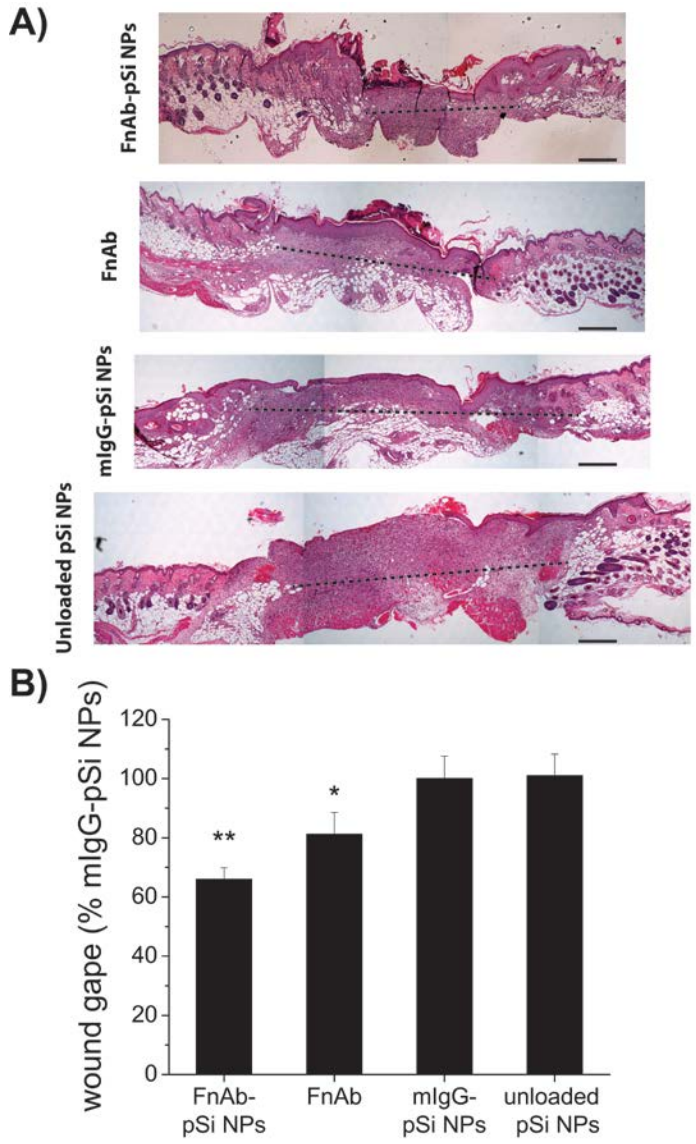


Figure 8: Microscopic analysis of excisional wound trial in diabetic mice. Wounds were treated with intradermal injections of FnAb-pSi NPs, FnAb alone, mIgG-pSi NPs or unloaded pSi NPs at the time of injury. Each wound was treated with the equivalent of 50 µg of FnAb or mIgG. Sections of day 7 wounds were stained with haematoxylin and eosin (A), with wound gape measured and presented as the % of mIgG-pSi NPs (B). The dashed lines in panel a show the width of the wounded dermis in each tissue section. Each treatment group contained six mice, with two wounds per mouse. Images in (A) were representative of each treatment group. * $P < 0.05$, ** $P < 0.005$ compared to mIgG-pSi NP treated controls. Scale bar is 100 µm.

3.6. pSi-loaded FnAbis protected from proteases

To determine if proteases are able to digest antibody loaded into the pores of the pSi NPs, FnAb-pSi NPs were transiently incubated with pepsin, a protease known to fragment IgG antibodies. pSi NPs were rinsed to remove residual pepsin, then an antibody release experiment was performed over 7 d, with antibody containing supernatant decanted each day for analysis. At each time point, FnAb released from pepsin-treated FnAb-pSi NPs was 150 kDa, indicating the antibody was structurally intact, the same as observed for FnAb-pSi NPs not treated with pepsin (**Figure 9**). A weak band corresponding to pepsin was observed in the day 0 sample, but not any of the latter time points, suggesting most pepsin was effectively removed prior to commencing the release experiment. Free FnAb incubated with pepsin, using the same digestion conditions the pSi NPs were exposed to, led to the complete absence of 150 kDa bands on the gel, indicating digestion conditions were sufficient to completely digest unprotected FnAb. Similar results were obtained for pSi MPs (**Figure S5**).

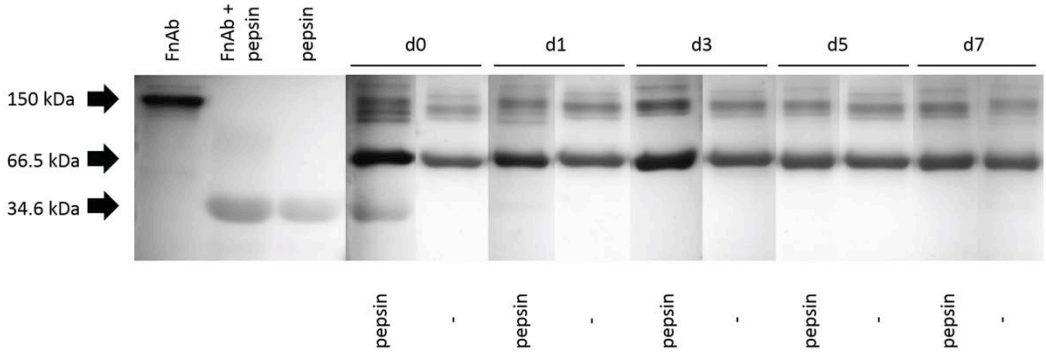


Figure 9: Protease treatment on FnAb-pSi NPs. FnAb-pSi NPs were transiently incubated with or without pepsin at 37 ºC, then incubated for 7 d at 25ºC, with supernatants decanted daily for analysis of structural integrity. Samples were run on SDS-PAGE gels and then coomassie-stained. Structurally intact FnAb was identified as 150 kDa. Albumin, identified as a 66.5 kDa band, was added to the supernatant during the release experiment to assist with the stability of the released antibody. Pepsin was identified as the 34.6 kDa band on the gel. Free FnAb, incubated with and without pepsin, was also run on the gel, (as positive and negative controls) along with free pepsin.

4. Discussion

pSi is being exploited for applications in drug delivery including in several preclinical and clinical settings.[11, 41] A particularly suitable format of pSi for drug delivery are MPs that are fabricated to the desired size from “free-standing” membranes of pSi by sonication[42] or other mechanical forces, such as ball milling.[43] In our earlier study, pSi-MPs loaded with Infliximab were used to neutralise TNF-α in wound fluid,[27] highlighting the usefulness of pSi as delivery vehicle for wound healing applications.

pSi NPs are now becoming commonplace for biomedical applications with recent examples including work on the delivery of oligonucleotides[44] and small molecular drugs[45] among others.[46] pSi NPs are generated in a similar manner to pSi MPs, however, it is common to further nanostructure the pSi membrane with perforations, using a square etching waveform, before sonication or ball milling into nanoparticles.[47] Here, pSi NPs were evaluated as a drug delivery vehicle for chronic

wounds, in part due to their ease of fabrication, but also because they can be easily injected or further processed into bandages or gels for topical applications. Importantly, pSi NPs can also be loaded with large payloads of therapeutic antibodies, on average 268 µg per mg pSi NPs and up to 303 µg per mg pSi NPs. This corresponds to an approximately 4-fold higher loading than observed previously in pSi MPs,[27] possibly due to more efficient packing of the antibody.

pSi NPs degrade under physiological conditions,[48] releasing the antibody so it is available to neutralise its target antigen. Here, FnAb-pSi NPs incubated at 25 ºC, a similar temperature to the to the diabetic ulcer environment,[49] were found to release 86.3% of total loaded FnAb after 7 d, which is expected to be a suitable window for improved wound healing. This was higher than observed in pSi MPs loaded with Infliximab, where approximately 50% of total loaded antibody was released over an equivalent time frame, despite NPs being loaded with more antibody.[27] Using NPs will therefore allow less pSi to be administered to patients in a clinical setting than when using MPs.

As pSi degrades, silicic acid is the major breakdown product produced.[50] Previous studies have found that pSiis biocompatible, biodegradable and bioresorbable in animals[51] and pSi has now been used in human trials.[52] In the current study, the breakdown products of pSi, sodium metasilicate, had no detrimental effect on FnAb functionality. This agrees with our previous study where the functionality of the therapeutic antibody Infliximab was not affected by release from and degradation of pSi MPs.[27]

The nature of antibody-pSi binding is electrostatic[27] and it is important to carefully control the strength of this binding as damage can be caused to the protein structure, resulting in loss of activity.[53] To demonstrate that loaded antibody retained its functionality, a modified sandwich ELISA was performed, showing FnAb bound to pSi retained its ability to bind to the target antigen. Next, the FnAb detection ELISA was used to tested samples of supernatant decanted from FnAb-pSi NPs after incubation at 25 ºC. FnAb was found to be effectively released from pSi NPs into the supernatant and was able to bind to the Flii antigen target.

Scratch wounding assays and proliferation assays in cultured cells have previously shown increased wound closure and proliferation in response to FnAb treatment.[19] Here, these assays found FnAb retained its functionality, and was released at sufficient levels to have a physiological effect on cultured cells, indicating that loading densities of the particles were sufficiently high to be useful *in vitro*.

FnAb treatment of cultured cells has previously shown in numerous studies to increase wound closure and proliferation as measured by scratch wounding and proliferation assays.[19] These assays were utilised in the current study to evaluate whether the FnAb released from pSi NPs was structurally intact and without conformational change. Here, FnAb released from pSi NPs was shown to retain its functionality, and moreover was released at sufficient levels to have a physiological effect on cultured cells, indicating that loading densities of the particles were sufficiently high to be useful *in vitro*.

Mice are not an ideal model of dermal wound healing, as they are loose skinned and there is an elevated reliance on contraction compared to human skin.[54] However, mice are still widely used in dermal wound healing studies, allowing a number of incremental advances in the understanding of Flii's role in wound repair.[19, 22b, 23, 24b] For example, FnAb has been previously administered to acute incisional wounds in mice, showing improved wound appearance and increased wound closure.[19] In the current study, acute incisional wounds treated with a single dose of FnAb-pSi NP at the time of wounding showed a significant reduction in wound area and an increased rate of wound closure compared to untreated controls. Notably, the reduction in wound gape at day 7 was similar to those wounds treated with free FnAb in the absence of pSi NPs, providing important evidence that functional FnAb was successfully released from pSi NPs and into the wound environment. The improvement in wound healing indicated that the pSi NP pores were not blocked by wound fluid, which was a possible limitation of using pSi. No difference in wound gape at day 7 between mIgG-pSi NP, mIgG alone and unloaded pSi NP treated wounds was observed, indicating that pSi NPs alone have no effect on wound closure.

The repeated administration of low-dose STZ to healthy wild-type mice induces diabetes[55], leading to delayed wound closure[22a] and elevated protease concentration in wounds.[56] One study showed these mice having elevated matrix metalloproteinase (MMP)-9 protein levels in excisional wounds compared to those in healthy non-diabetic controls at both day 3 and at wound closure,[56] indicating a protease rich wound environment. As there is a lack of true chronic ‘non-healing’ wound models, STZ treated mice therefore provide a valuable *in vivo* model to evaluate whether pSi NPs improved the delivery of FnAb to protease rich wound environments. Here,

treatment with free FnAb accelerated the rate of wound closure compared to free mIgG treated controls, suggesting the diabetic wound environment did not completely degrade the administered antibody, and agreeing with a previous study.[22a] Importantly, delivering a single dose of FnAb-pSi NPs showed a further statistically significant improvement in the rate of wound healing compared to administering an equivalent dose of free FnAb alone. Using pSi NPs as a delivery vehicle therefore improves wound healing in STZ-treated wounds. No difference in wound area was seen between treatment with FnAb alone compared to FnAb and pSi NPs when added together (i.e. NPs were not loaded with antibody prior to administration), suggesting FnAb must be loaded into the pores to enhance wound closure.

A number of proteases are elevated in chronic wounds, including MMPs,[57] with one study showing ≥ 30-fold higher MMP activity in chronic than acute wounds.[58] MMP-3 and MMP-7 are reported to degrade IgG antibodies,[37, 59] therefore likely contributing to impaired efficacy of therapeutic antibodies in diabetic wounds. Experiments were therefore performed to determine whether pSi could actually protect the therapeutic antibody from proteases, providing a mechanism to explain the improved efficacy in diabetic wounds compared to when FnAb was administered alone. Here, FnAb-pSi NPs were incubated with pepsin under conditions that completely degrade FnAb alone. The subsequent release experiment showed that FnAb released from these particles had retained its structural integrity, thereby confirming that the pSi provides a protective environment from proteases.

In this work, we delivered pSi NPs loaded with FnAb by intradermal injection at the wound margin. Concurrent studies have showed that delivery of FnAb pSi NPs to incisional wounds in wild-type mice was as effective when delivered topically in a hydrogel as when administered intradermally (unpublished data). Although intradermal injection is not a practical mode of administration for the clinic it was performed in the current study as it was an effective method of delivering the drug to the wound margin. Our future plan is to further investigate a number of topical applications and also translating the delivery method into a dressing platform. We have taken significant strides towards this already (see **Figure S6** and **S7**) with animal trials soon to follow. It is expected that the dressings and further modification to the NPs could bring significant improvements to the ability of diabetic wounds to heal.

5. Conclusion

We demonstrate that pSi NPs have a high loading capacity for FnAb and can extend antibody release for 7 d *in vitro*. The released FnAb was active and detectable by ELISA. The released FnAb was also active as determined by *in vitro* assays in keratinocytes, and when injected *in vivo* the loaded pSi NPs were able to improve the wound healing of both incisional acute wounds and excisional diabetic wounds. Importantly, the pSi NPs were able to impart protection to the FnAb stored within the pores as demonstrated by protease experiments. It is envisaged that pSi NPs can be incorporated into wound dressings materials and deliver FnAb to wound fluid in order to improve chronic wound healing.

Acknowledgements

The authors would like to acknowledge the support of the Australian Government's Cooperative Research Centre Programme. [$]Dr. Chris T. Turner and Dr. Steven J. P. McInnes contributed equally to this work.

Received: ((will be filled in by the editorial staff))
Revised: ((will be filled in by the editorial staff))
Published online: ((will be filled in by the editorial staff))

[1] W. M. Innovation, 2013-14.
[2] R. Nunan, K. G. Harding, P. Martin, *Dis. Model Mech.* **2014**, 7, 1205.
[3] N. Singh, D. G. Armstrong, B. A. Lipsky, *JAMA* **2005**, 293, 217.
[4] F. Quondamatteo, *Cell Tissue Res.* **2014**, 355, 1.
[5] C. B. Payne, *Med. J. Aust.* **2000**, 173, 352.
[6] G. E. Reiber, L. Vileikyte, E. J. Boyko, M. del Aguila, D. G. Smith, L. A. Lavery, A. J. Boulton, *Diabetes Care* **1999**, 22, 157.
[7] C. T. Turner, S. J. P. McInnes, A. J. Cowin, *Wound Practice Res.* **2015**, 23, 16.
[8] a) L. Canham, *Properties of porous silicon*, Short Run Press, London 2006; b) J. K. Tessmar, A. M. Göpferich, *Adv. Drug Delivery Rev.* **2007**, 59, 274.
[9] a) S. J. P. McInnes, E. J. Szili, S. A. Al-Bataineh, J. Xu, M. E. Alf, K. K. Gleason, R. D. Short, N. H. Voelcker, *ACS Appl. Mater. Interfaces* **2012**, 4, 3566; b) S. J. P. McInnes, H. Thissen, N. R. Choudhury, N. H. Voelcker, *J. Colloid Interface Sci.* **2009**, 332, 336.
[10] a) S. D. Alvarez, A. M. Derfus, M. P. Schwartz, S. N. Bhatia, M. J. Sailor, *Biomaterials* **2009**, 30, 26; b) L. Canham, R. Aston, *Phys. World* **2001**, 27; c) L. T. Canham, *Adv. Mater.* **1995**, 7, 1033.
[11] S. P. Low, N. H. Voelcker, L. T. Canham, K. A. Williams, *Biomaterials* **2009**, 30, 2873.
[12] L. Cheng, E. Anglin, F. Cunin, D. Kim, M. J. Sailor, I. Falkenstein, A. Tammewar, W. R. Freeman, *Brit. J. Ophthal.* **2008**, 92, 705.
[13] L. M. Bimbo, M. Sarparanta, H. l. A. Santos, A. J. Airaksinen, E. Mäkilä, T. Laaksonen, L. Peltonen, V.-P. Lehto, J. Hirvonen, J. Salonen, *ACS Nano* **2010**, 4, 3023.
[14] E. J. Szili, A. Jane, S. P. Low, M. Sweetman, P. Macardle, S. Kumar, R. S. C. Smart, N. H. Voelcker, *Sens. Actuators, B* **2011**, 160, 341.
[15] M. J. Sailor, J.-H. Park, *Adv. Mater.* **2012**, 24, 3779.
[16] a) F. S. H. Krismastuti, S. Pace, E. Melville, A. J. Cowin, T. R. Dargaville, N. H. Voelcker, *Aust. J. Chem.* **2013**, 66, 1428; b) S. Pace, R. B. Vasani, F. Cunin, N. H. Voelcker, *New J. Chem.* **2012**, 37, 228.
[17] A. M. Rossi, L. Wang, V. Reipa, T. E. Murphy, *Biosens. Bioelectron.* **2007**, 23, 741.
[18] a) J. S. Andrew, E. J. Anglin, E. C. Wu, M. Y. Chen, L. Cheng, W. R. Freeman, M. J. Sailor, *Adv. Funct. Mater.* **2010**, 20, 4168; b) J. Rytkönen, P. Arukuusk, W. Xu, K. Kurrikoff, Ü. Langel, V.-P. Lehto, A. Närvänen, *Mol. Pharmaceutics* **2014**, 11, 382; c) J. Salonen, L. Laitinen, A. Kaukonen, J. Tuura, M. Bjorkqvist, T. Heikkila, K. Vaha-Heikkila, J. Hirvonen, V. P. Lehto, *J. Control. Rel.* **2005**, 108, 362.

[19] A. Cowin, D. Adams, X. Strudwick, H. Chan, J. Hooper, G. Sander, T. Rayner, K. Matthaei, B. Powell, H. Campbell, *J Pathol.* **2007**, 211, 572.
[20] Z. Kopecki, A. J. Cowin, *Int. J. Biochem. Cell Biol.* **2008**, 40, 1415.
[21] Defilippi P, Olivo C, Venturino M, Dolce L, Silengo L, Tarone G, *Microsc. Res. Tech.* **1999**, 47, 67.
[22] a) N. Ruzehaji, R. Grose, D. Krumbiegel, H. Zola, P. Dasari, H. Wallace, M. Stacey, R. Fitridge, A. J. Cowin, *Eur J Dermatol.* **2012**, 22, 740; b) N. Ruzehaji, Z. Kopecki, E. Melville, S. L. Appleby, C. S. Bonder, R. M. Arkell, R. Fitridge, A. J. Cowin, *Diabetologia* **2014**, 57, 402.
[23] D. H. Adams, N. Ruzehaji, X. L. Strudwick, J. E. Greenwood, H. D. Campbell, R. Arkell, A. J. Cowin, *Brit. J. Dermatol.* **2009**, 161, 326.
[24] a) J. E. Jackson, Z. Kopecki, D. H. Adams, A. J. Cowin, *Wound Repair Regen.* **2012**, 20, 523; b) Z. Kopecki, N. Ruzehaji, C. Turner, H. Iwata, R. J. Ludwig, D. Zillikens, D. F. Murrell, A. J. Cowin, *J. Invest. Dermatol.* **2013**, 133, 1008.
[25] R. W. Tarnuzzer, G. S. Schultz, *Wound Rep. Reg.* **1996**, 4, 321.
[26] S. Schreml, R.-M. Szeimies, S. Karrer, J. Heinlin, M. Landthaler, P. Babilas, *JEADV* **2010**, 24, 373.
[27] S. J. P. McInnes, M. J. I. A. Leccardi, C. T. Turner, Y. Irani, A. J. Cowin, K. A. Williams, N. H. Voelcker, *J. Mater. Chem. B* **2015**, 3, 4123.
[28] a) G. Y. Berguig, A. J. Convertine, S. Frayo, H. B. Kern, E. Procko, D. Roy, S. Srinivasan, D. H. Margineantu, G. Booth, M. C. Palanca-Wessels, D. Baker, D. Hockenbery, O. W. Press, P. S. Stayton, *Molecular Therapy* **2015**, 23, 907; b) J. Fu, C. Yu, L. Li, S. Q. Yao, *J. Am. Chem. Soc.* **2015**, 137, 12153.
[29] W. Armarego, D. Perrin, *Purification of laboratory chemicals*, Butterworth-Heinemann, 1996.
[30] J. Wegener, C. R. Keese, I. Giaever, *Exp. Cell Res.* **2000**, 259, 158.
[31] I. H. Heijink, S. M. Brandenburg, J. A. Noordhoek, D. S. Postma, D.-J. Slebos, A. J. M. v. Oosterhout, *Eur. Respir. J.* **2010**, 35, 894.
[32] Moura LIF, Dias AMA, Suesca E, Casadiegos S, Leal EC, Fontanilla MR, Lina Carvalho, Hermínio C. de Sousa, E. Carvalho, *Biochimica et Biophysica Acta* **2014**, 1842, 32.
[33] M. S. Johnson, J. M. Ryals, D. E. Wright, *Pain* **2008**, 140, 35.
[34] J. Michaels, S. S. Churgin, K. M. Blechman, M. R. Greives, S. Aarabi, R. D. Galiano, G. C. Gurtner, *Wound Rep. Reg.* **2007**, 15, 665.
[35] J.-D. Luo, Y.-Y. Wang, W.-L. Fu, J. Wu, A. F. Chen, *Circulation* **2004**, 110, 2484.
[36] R. D. Lillie, H. M. Fullmer, *Histopathologic technic and practical histochemistry*, McGraw Hill Book Company, New York 1976.
[37] A. J. H. Gearing, S. J. Thorpe, K. Miller, M. Mangan, P. G. Varley, T. Dudgeon, G. Ward, C. Turner, R. Thorpe, *Immunol. Lett.* **2002**, 81, 41.
[38] C. T. Turner, J. M. Waters, J. E. Jackson, R. M. Arkell, A. J. Cowin, *Experimental Dermatology* **2015**, 24, 692.
[39] a) K. L. Pong, S. C. Chen, K. W. Cheah, *Solid State Commun.* **1996**, 99, 887; b) F. X. Qiu, P. P. Li, D. Y. Yang, *eXPRESS Polymer Letters* **2007**, 1, 150; c) E. Kondoha, T. Asano, A. Nakashima, M. Komatu, *J. Vac. Sci. Technol. B* **2000**, 18, 1276.
[40] T. J. Higuchi, *Pharm. Sci.* **1961**, 50, 847.
[41] a) J. Chhablani, A. Nieto, H. Hou, E. C. Wu, W. R. Freeman, M. J. Sailor, L. Cheng, *Invest. Ophthalmol. Visual Sci.* **2013**, 54, 1268; b) K. Zhang, S. L. E. Loong,

S. Connor, S. W. K. Yu, S.-Y. Tan, R. T. H. Ng, K. M. Lee, L. Canham, P. K. H. Chow, *Clin. Cancer Res.* **2005**, 11.
[42] a) J. R. Dorvee, A. M. Derfus, S. N. Bhatia, M. J. Sailor, *Nat. Mater.* **2004**, 3, 896; b) J. Link, M. J. Sailor, *PNAS* **2003**, 100, 10607; c) J. C. Thomas, C. Pacholski, M. J. Sailor, *Lab Chip* **2006**, 6, 782; d) E. C. Wu, J.-H. Park, J. Park, E. Segal, F. Cunin, M. J. Sailor, *ACS Nano* **2008**, 2, 2401.
[43] M. G. Donato, M. A. Monaca, G. Faggio, L. De Stefano, P. H. Jones, P. G. Gucciardi, O. M. Marago, *Nanotechnology* **2011**, 22, 505704.
[44] M. H. Kafshgari, B. Delalat, W. Y. Tong, F. J. Harding, M. Kaasalainen, J. Salonen, N. H. Voelcker, *Nano Research* **2015**, 8, 2033.
[45] a) J. Ryu, B. Cho, H.-G. Woo, S. Cho, H. Sohn, *J. Nanosci. Nanotechnol.* **2013**, 13, 157; b) E. Secret, K. Smith, V. Dubljevic, E. Moore, P. Macardle, B. Delalat, M.-L. Rogers, T. G. Johns, J.-O. Durand, F. Cunin, N. H. Voelcker, *Adv. Healthcare Mater.* **2013**, 2, 718.
[46] a) H. Chanseok, L. Jungkeun, Z. Hongmei, H. Soon-Sun, L. Chongmu, *Nanoscale Res. Lett.* **2011**, 6, 321; b) D. Liu, L. M. Bimbo, E. Mäkilä, F. Villanova, M. Kaasalainen, B. Herranz-Blanco, C. M. Caramella, V.-P. Lehto, J. Salonen, K.-H. Herzig, J. Hirvonen, H. A. Santos, *J. Control. Rel.* **2013**, 170, 268.
[47] a) M. H. Kafshgari, A. Cavallaro, B. Delalat, F. J. Harding, S. J. P. McInnes, E. Mäkilä, J. Salonen, K. Vasilev, N. H. Voelcker, *Nanoscale Res. Lett.* **2014**, 9, 333; b) L. Russo, F. Colangelo, R. Cioffi, I. Rea, L. D. Stefano, *Materials* **2011**, 4, 1023; c) Z. Qin, J. Joo, L. Gu, M. J. Sailor, *Part. Part. Syst. Charact.* **2014**, 31, 252.
[48] a) E. J. Anglin, L. Cheng, W. R. Freeman, M. J. Sailor, *Adv. Drug Deliv. Rev.* **2008**, 60, 1266; b) S. P. Low, K. A. Williams, L. T. Canham, N. H. Voelcker, *Biomaterials* **2006**, 27, 4538.
[49] P.-C. Sun, H.-D. Lin, S.-H. E. Jao, Y.-C. Ku, R.-C. Chan, C.-K. Cheng, *Diabetes Res. Clin. Pract.* **2006**, 73, 41.
[50] S. Anderson, H. Elliott, D. Wallis, L. Canham, J. Powell, *Phys. Status Solidi A* **2003**, 197, 331.
[51] J. H. Park, L. Gu, G. von Maltzahn, E. Ruoslahti, S. N. Bhatia, M. J. Sailor, *Nat. Mater.* **2009**, 8, 331.
[52] L. Canham, D. Ferguson, in *Handbook of Porous Silicon*, (Ed: L. Canham), Springer International Publishing, Switzerland 2014.
[53] K. L. Jarvis, T. J. Barnes, C. A. Prestidge, *Langmuir* **2010**, 26, 14316.
[54] G. C. Gurtner, S. Werner, Y. Barrandon, M. T. Longaker, *Nature* **2008**, 453, 314.
[55] V. Kolb-Bachofen, S. Epstein, U. Kiesel, H. Kolb, *Diabetes* **1988**, 37, 21.
[56] Liane I. F. M., Ana M. A. D., Edward S., Sergio C., Ermelindo C. L., Marta R. F., Lina C., Hermínio C. de S., Eugénia C., *Biochim. Biophys. Acta* **2014**, 1842, 32.
[57] S. M. McCarty, S. L. Percival, *Adv. Wound Care* **2012**, 2, 438.
[58] N. J. Trengove, M. C. Stacey, S. MacAuley, N. Bennett, J. Gibson, F. Burslem, G. Murphy, G. Schultz, *Wound Rep. Reg.* **1999**, 7, 442.
[59] R. J. Brezski, R. E. Jordan, *mAbs* **2010**, 2, 212.